32nd Annual International Conference of the IEEE EMBS
Buenos Aires, Argentina, August 31 - September 4, 2010

Decoupled External Forces in a Predictor-Corrector Segmentation Scheme for LV Contours in Tagged MR Images

Jaume Garcia-Barnes, Albert Andaluz, Francesc Carreras and Debora Gil

Abstract— **Computation of functional regional scores requires proper identification of LV contours. On one hand, manual segmentation is robust, but it is time consuming and requires high expertise. On the other hand, the tag pattern in TMR sequences is a problem for automatic segmentation of LV boundaries.**

We propose a segmentation method based on a predictor-corrector (Active Contours - Shape Models) scheme. Special stress is put in the definition of the AC external forces. First, we introduce a semantic description of the LV that discriminates myocardial tissue by using texture and motion descriptors. Second, in order to ensure convergence regardless of the initial contour, the external energy is decoupled according to the orientation of the edges in the image potential. We have validated the model in terms of error in segmented contours and accuracy of regional clinical scores.

I. INTRODUCTION

A main feature of heart diseases is that they decrease the blood supply at specific areas of the heart, leading to abnormal regional wall motion patterns. It follows that wall motion analysis is crucial for an early diagnosis. Computation of function parameters for regional wall motion abnormalities assessment requires both, accurate motion extraction and segmentation of myocardial boundaries for the definition of myocardial segments.

Tagged Magnetic Resonance (TMR) [1] is the reference image modality for evaluating the local mechanical properties of the myocardium. TMR "overlays" a grid-like pattern which deformation along cardiac cycle allows visualization and measurement of intramural deformation. Although there is a large variety of methods for LV segmentation for standard magnetic resonance images, they fail to give the expected results in TMR sequences due to the tag pattern. On one hand, the tag pattern generates high gradients which causes the tags to have the same local properties as LV contours. On the other hand, at initial time , that is, End-Diastole, blood pool is also tagged and the endocardium can not be outlined. It follows that, automatic and semi-automatic segmentation of the myocardium has been seldom tackled in TMR sequences so far. In [2], gray-scale morphological operations are used to separate non-tagged blood-filled regions from the tagged myocardium regions. Recent works use texture descriptors in order to model the appearance of tags. In [3], [4] Metaxas *et al.* have addressed the problem from the perspectives of shape, intensity and appearance modeling. More recently [5], the same authors have used AdaBoost for combining appearance, motion and shape constrains. Finally, in [6], [7] LV contours are segmented by applying some texture analysis in order to remove tags, followed by the use of deformable models (deformable template in [6], active contours in [7]) in the obtained untagged images.

Although the myocardium is the only structure in TMR sequences presenting a clear dynamical behaviour, the role of motion is mainly restricted to tracking an initial segmentation along the whole cycle [5], [8]. By using only texture information for defining LV contours, segmentations might include surrounding tagged tissue. Another critical point is the initialization of the Active Contours (AC), which should be close enough to the target boundaries. Moreover, in the case of the LV, endocardial features may attract the epicardial contour and vice versa. In order to reduce the impact of initial contours, some authors [9]–[11] consider directional information by inhibiting the influence of image contours not oriented along the snake.

In this work we present a method for the segmentation of the LV contours in TMR sequences at End Diastole (ED). Our proposed method consists of a preprocessing stage that discriminates myocardial tissue by using a semantic description that combines texture and motion. Texture serves for eliminating the tagging pattern and by, considering motion, LV contours are better discriminated from adjacent tagged tissue (like the liver). Lastly, the segmentation stage is implemented as a combination of AC and Shape Models (SM) in a predictor-corrector scheme [11]. In order to avoid convergence to local minima, the predictor-corrector scheme is driven by multiple external forces decoupling the geometry of contours. This way, each node of the AC is only influenced by one external force according to the orientation of its normal direction. This strategy provides robustness to the process avoiding initialization near the target boundaries and, consequently relaxes the need for user interaction. Besides, the use of a SM ensures that the AC only deforms according to set of valid shapes previously learnt.

We have evaluated the performance of our method at Basal, Mid and Apical Short Axis (SA) slices in a set of 21 healthy volunteers in terms of error in the position of automated contours and accuracy of regional clinical scores (rotation). For both LV walls (epicardium and endocardium), the average error is below 2 pixels in all levels. This error does not introduce a significant bias in (segmental and

This work was supported by the Spanish projects PI071188, TIN2009-13618 and CONSOLIDER INGENIO 2010 (CSD2007-00018). The last author has been supported by The Ramon y Cajal Program.

J. Garcia-Barnes and D. Gil are with Computer Vision Center and Department of Computer Science, Univ. Autonoma de Barcelona, Bellaterra, Spain. jaumegb,debora@cvc.uab.es

A. Andaluz is with Computer Vision Center,Univ. Autonoma de Barcelona, Bellaterra, Spain. aandaluz@cvc.uab.es

F. Carreras is with the Hospital de Sant Pau, Barcelona, Spain.

global) rotation, which validates our method for clinical use.

II. A Decoupled Predictor-Corrector Scheme

Active Contours or *Snakes* [12] are elastic curves, $\mathcal{S}(u) = (x(u), y(u)),\ u \in [0,1]$, that minimize the following energy functional:

$$E(\mathcal{S}(u)) = \int_0^1 E_{int}(\mathcal{S}(u)) + E_{ext}(\mathcal{S}(u))\, du \qquad (1)$$

The internal energy E_{int} controls the regularity of the curve, while the external one E_{ext} is computed from images and drives the snake towards the boundaries of interest. Solutions to (1) are given by the following iterative scheme:

$$\mathcal{S}^{t+1} = (A + Id)^{-1}\ \left(\mathcal{S}^t - \nabla E_{ext}(S^t)\right) \qquad (2)$$

where A is the stiffness matrix encoding the first and second derivatives of the curve S^t, Id the identity matrix and ∇ the gradient operator.

Shape Models [13] incorporate a previously learned model of the preferred shape for the target structure. A common approach for statistical modelling of shape is Principal Component Analysis (PCA), computed for a set of M landmarks located on contours in a set of training images. Landmarks are sampled in order to ensure that they represent the same anatomical position and are aligned by procrustes analysis [14] in order to remove affinities. The concatenation of the (2D) coordinates of all aligned landmarks, $\{(x_m^n, y_m^n)\}_{m=1}^M$ constitutes the observation for the n-th individual:

$$X^n = (x_1^n, \ldots, x_M^n, y_1^n, \ldots, y_M^n) \qquad (3)$$

PCA analysis is given by the average, $\bar{X}$, and the covariance matrix, C, of all observations. The eigenvectors $(\phi_n)_{n=1}^{2M}$ of C encode the modes of variation of the model and the eigenvalues $\lambda_1 \geq \cdots \geq \lambda_{2M}$, the relevance of such mode.

The shape model for a new individual, X, codified with M landmarks is defined by projecting it into the subspace spanned by the first d eigenvectors:

$$X \approx \bar{X} + \Phi\Phi^T(X - \bar{X}) = \bar{X} + \Phi b \qquad (4)$$

where $\Phi = (\phi_1|\phi_2|\cdots|\phi_d)$ is the column matrix of the first d eigenvectors and $b = (b_1, \ldots, b_d)$ is the shape parameter given by the projection matrix $\Phi^T(X - \bar{X})$.

In our model, shape correction is applied to an active contour by using a predictor-corrector scheme [11] that yields a controlled evolution of the snake.

A. Predictor-Corrector Scheme

Given the snake at time t we predict its next position by applying (2). After this, we correct the estimation by looking for the most similar valid shape given by our shape model (4) . Since the shape correction constrain might impair the evolution of the prediction step, it is only applied every Q iterations.

The initial snake is given by the average shape, centered at images and oriented according to the superior RV-LV junction of images. In order to preserve the initial distribution of landmarks, the prediction stage only takes into account the component of external forces, normal to the current snake, $\nabla E_{ext}^{\perp} = \langle \vec{n}, \nabla E_{ext} \rangle \vec{n}$, for $\vec{n}$ the normal vector to the snake and $\langle \cdot, \cdot \rangle$ the scalar product.

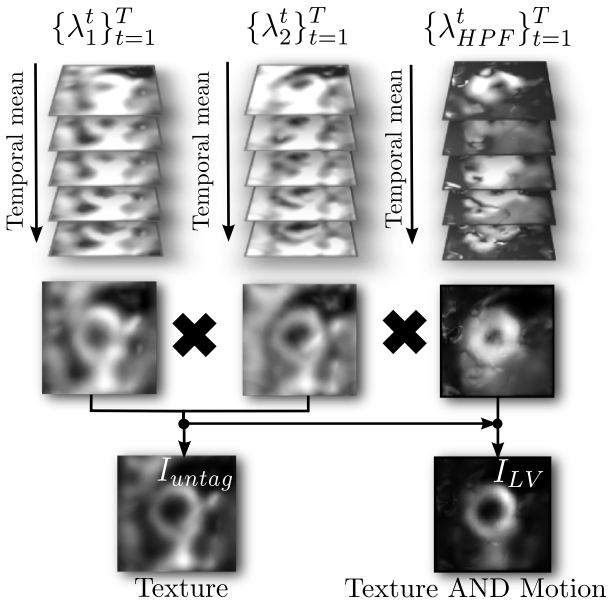

Fig. 1. Tags and surrounding tissue filtering. Texture information removes most of the tags (I_{untag}). However, by incorporating motion information the filtering is extendend to the surrounding tissue (I_{LV}).

Notice that the convergence of our predictor-corrector scheme still depends on E_{ext}. For this reason, we propose a semantic description of myocardial tissue and a decoupling of E_{ext} influence, in order to avoid premature convergence to local minima.

B. Semantic Description of Myocardial Tissue

Myocardial tissue in TMR can be semantically described as those parts of the image, tagged along systole, which experience a significant deformation along the systolic cycle, relative to the surrounding tagged tissue.

The tagged pattern is modeled by the response to two Gabor filter banks, tailored to each tag direction. The response of each filter bank produces a complex image, whose phase is related to tissue motion [15]. Additionally, the amplitude indicates which areas of the image present a reliable tag pattern. Thus, it detects, for each frame, the tagged tissue. Finally, motion is detected by the magnitude of the dense motion field provided by the tracker HPF [15].

In order to obtain a single measure of tagging pattern and motion, Gabor amplitudes and motion vector magnitudes for all frames should be combined. Since the values obtained for a given pixel might not correspond to the same anatomical point, especially at moving areas, motion should be compensated first. We use HPF to backtrack any quantity, either amplitudes or module, to the first frame. The Gabor amplitudes and HPF magnitude backtracked to the 1st frame will be denoted by $\{\lambda_1^t\}_{t=1}^T, \{\lambda_2^t\}_{t=1}^T$ and $\{\lambda_{HPF}^t\}_{t=1}^T$, where the superindex represents the sequence frame. The average of $\{\lambda_1^t\}_{t=1}^T, \{\lambda_2^t\}_{t=1}^T$ and $\{\lambda_{HPF}^t\}_{t=1}^T$

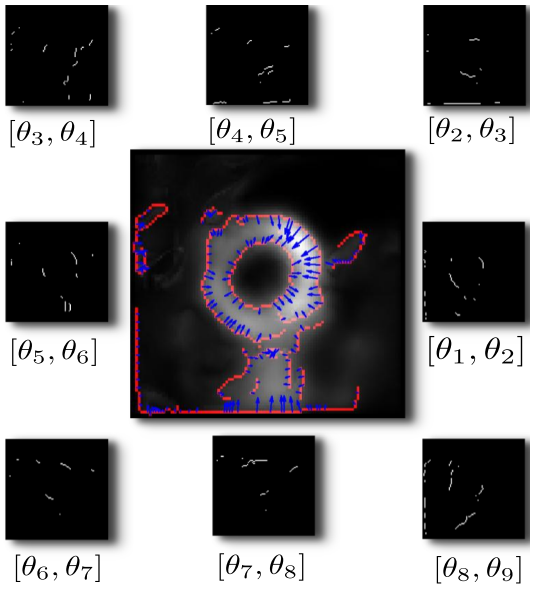

Fig. 2. Partition of the contours detected in I_{LV} (in red) according to the orientation of ∇I_{LV} (in blue). In this graphic, 8 sets have been considered. Each set induces a distance map $d_{[\theta_k,\theta_{k+1}]}$ that contributes to a term of the external energy.

for all frames reflects, respectively, persistence of tagging pattern and presence of any motion along the cardiac cycle. The condition $Texture\ AND\ Motion$ is formulated by the product of the three averages:

$$I_{LV} = \left(\frac{1}{T}\sum_t \lambda_1^t\right)\left(\frac{1}{T}\sum_t \lambda_2^t\right)\left(\frac{1}{T}\sum_t \lambda_{HPF}^t\right) \quad (5)$$

Figure 1 sketches the process of obtaining I_{LV}. The map I_{LV} represents the likelihood of belonging to the left ventricular area. It is suitable for defining any standard snake potential, either based on its gradient or on distance maps to its edges. In our case we use the latter.

C. Multiple Directional External Forces

In order to endow the predictor snake with independence from the initial contour, we consider that each snaxel should be only influenced by those image edges having a structural configuration similar to the snake at that point. For this reason, we split the edges of I_{LV} according to its orientation, given by the angle $\theta \in [0, 2\pi]$ of the gradient ∇I_{LV}) (see Figure 2). Next, we consider a separate distance map for each segment. The same angular partition is considered for the current snake, so that each snake segment only evolves according to the distance map presenting similar orientation.

Let $\theta_k = (2(k-1)\pi)/K$ be a uniform partition of the interval $[0, 2\pi]$ and $d_{[\theta_k,\theta_{k+1}]}$ the distance map to I_{LV} edges oriented towards $[\theta_k, \theta_{k+1}]$. The external energy is defined as the disjoint combination of all $d_{[\theta_k,\theta_{k+1}]}$, that is:

$$E_{ext}(\mathcal{S}) = \sum_{k=1}^{K} \chi_{[\theta_k,\theta_{k+1}]}(\mathcal{S})\ d_{[\theta_k\theta_{k+1}]}(\mathcal{S}) \quad (6)$$

for $\chi_{[\theta_k,\theta_{k+1}]}$ the characteristic function given by:

$$\chi_{[\theta_k,\theta_{i+k}]}(\mathcal{S}) = \begin{cases} 1, & \theta(\vec{n}) \in [\theta_k, \theta_{k+1}] \\ 0, & otherwise \end{cases} \quad (7)$$

where $\theta(\vec{n})$ is the angle of the normal vector to $\mathcal{S}$.

III. Results

Three different SM have been learnt for Base (B), Mid (M) and Apex (A). For each SM, we have considered 47 MR standard (**tag-free**) images at ED where the blood pool is visible. Next, 10 landmarks sampled on the epicardium and endocardium (20 landmarks in total) have been manually selected. Landmarks have been sampled clockwise starting at the superior LV-RV septal junction, first for the epicardium and then for the endocardium. The PCA-based SM is given by the 10 first modes of variation which retain approximately a 97% of the total variation in the three cases. Regarding the AC and the predictor-corrector scheme parameters, we have considered $K = 8$ and $Q = 5$ respectively, since they provide a good trade-off between accuracy and complexity in the first case and accuracy and speed in the second.

We have validated our method (for each of the 3 levels) in a set of 21 TMR sequences obtained from healthy volunteers, by addressing the following issues:

- **Segmentation error.** Segmentation error is given by the Euclidean distance between automated contours and manual segmentations carried out by a clinical expert. The average for all contour pixels indicates the overall contour accuracy in a single image. Epicardial and endocardial LV walls have considered separately.
- **Accuracy of regional clinical scores.** Since the ultimate goal of LV contours segmentation is computing regional scores of the LV function, we have explored the impact of inaccurate segmentations in the computation of some scores. In particular, global and regional rotation obtained over automated LV domain segmentations has been compared to the values obtained by manually segmenting LV contours.

Figure 3 shows segmented LV contours using our method (red dashed lines) and manually traced (green solid lines) for basal, mid and apical levels. In order to provide a better visualization, initial contours (at End-Diastole) have been evolved using HPF [15] and are shown in the second frame where the blood pool is visible. Table I reports the statistical ranges (given by the average $\pm$ the standard deviation for the 21 cases) for contours error (1st column), global rotation (2nd column) and segmental rotation (3rd-8th columns) at base, mid and apex. Segmental rotation has been computed using AHA segments. The average error for epicardium and endocardium is similar and stays below 2 pixels (pixel spacing: 1.56 mm^2/px) for all levels (B, M and A). Given that global rotation considers all points inside LV borders, it is more stable against segmentation errors than segmental rotation. Regarding error ranges, at base and mid cuts, both, global and segmental present a stable behavior with average error under 0.5 degrees. For apical cuts, there is a significant

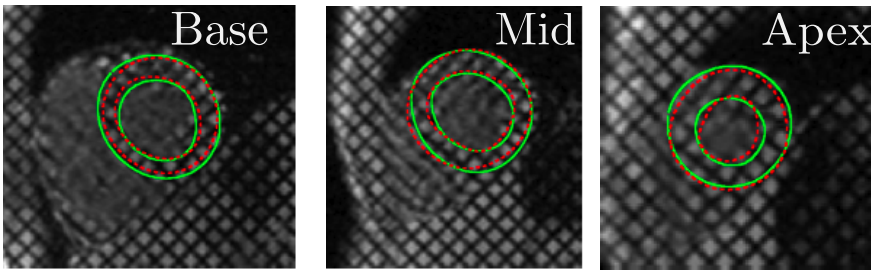

Fig. 3. Segmentation Results for base, mid and apex. For a better visualization, results are shown in the second frame where the blood pool is visible. Both, manual (green bold) and automatic (red dashed) contours have been updated using HPF motion field.

TABLE I
ERROR RANGES

	Contours	Global	Seg1	Seg2	Seg3	Seg4	Seg5	Seg6
B	1.60 ± 0.70	0.15 ± 0.11	0.45 ± 0.3	0.40 ± 0.20	0.40 ± 0.21	0.46 ± 0.25	0.32 ± 0.16	0.34 ± 0.25
M	1.90 ± 0.90	0.16 ± 0.15	0.39 ± 0.25	0.44 ± 0.30	0.59 ± 0.62	0.35 ± 0.19	0.35 ± 0.21	0.38 ± 0.26
A	1.74 ± 0.92	0.53 ± 0.49	0.70 ± 0.52	1.27 ± 1.40	0.60 ± 0.48	0.59 ± 0.44	-	-

increase in rotation errors, although they stay below 1 degree. We believe this decrease in accuracy is caused by bad propagation of errors. Furthermore, the tight enclosing of the apex to surrounding tissue is prone to interfere in motion computations.

IV. CONCLUSIONS

Segmentation of LV contours using AC in TMR sequences is a difficult task compared to other imaging modalities. In addition to premature convergence to local minima, the grid pattern hinders common external energies. This problem is usually solved by an initial contour close to the target structure. Concerning tags, current techniques remove them but still include adjacent tissue.

In this paper we present a predictor-corrector segmentation scheme that combines AC and SM. The proposed methodology contributes to the segmentation of LV contours in two ways. First, we describe the myocardial tissue in terms of tagging pattern and motion along cardiac cycle. By including motion, LV is discriminated from adjacent tagged tissue and defines a likelihood map, which is suitable to derive standard external energies. Second, in order to avoid dependency on the initial contour, we consider multiple external forces decoupling the geometry of contours. In this manner, each point in the active contour is attracted by the image contour presenting the most similar geometric structure.

Results show promising accuracy in contour aproximation, with an average error below 2 pixels. Although in this study only one expert was involved, we are currently retrieving additional data in order to account inter-observer variability and ensure that automatic segmentations are valid for clinical practice. We also believe pathological cases should be included in the SM, to avoid being restricted to healthy cases. An interesting conclusion from our experiments is that LV rotation,either global or segmental, is stable against segmentation errors. Therefore, future work will focus on the stability of other regional scores, to establish which ones are more robust in the field of segmentation variability.

REFERENCES

[1] L. Axel and L. Dougherty, "Mr imaging of motion with spatial modulation of magnetization," *Radiology*, vol. 171, pp. 841–845, 1989.
[2] A. Montillo, D. Metaxas, and L. Axel, "Automated segmentation of the left and right ventricles in 4d cardiac spamm images," in *MICCAI2002*, 2002, pp. 620–633.
[3] X. Huang, Z. Li, and D. Metaxas, "Learning coupled prior shape and appearance models for segmentation," in *Proc. Med. Image Comput. Computer-Assisted Intervention (MICCAI)*, vol. 1, 2004, pp. 60–69.
[4] Z. Qian, D. Metaxas, and L. Axel, "A learning framework for the automatic and accurate segmentation of cardiactagged mri images," in *Proceedings Of CVIBA Workshop, In Conjuction with ICCV*, ser. LNCS, vol. 3765, 2005, pp. 93–102.
[5] ——, "Learning methods in segmentation of cardiac tagged mri," in *Proceedings of ISBI*, 2007, pp. 688–691.
[6] J. Milles, A. van Susteren, T. Arts, P. Clarysse, and P. Croisille, "Automatic 2d segmentation of the left ventricle in tagged cardiac mri usingmotion information," in *Proceedings of the 2004 IEEE International Symposium on Biomedical Imaging:From Nano to Macro (ISBI)*, 2004, pp. 153–156.
[7] A. Histace, B. Matuszewski, and Y. Zhang, "Segmentation of myocardial boundaries in tagged cardiac mri using activecontours: a gradient-based approach integrating texture analysis," *Journal of Biomedical Imaging*, pp. 1–8, 2009.
[8] Z. Qian, D. Metaxas, and L. Axel, "Boosting and nonparametric based tracking of tagged mri cardiac boundarie," in *Proc. Med. Image Comput. Computer-Assisted Intervention (MICCAI)*, vol. 1, 2006, pp. 636–644.
[9] P. Radeva, J. Serrat, and E. Marti, "A snake for model-based segmentation," in *Proc. Fifth International Conference on Computer Vision (ICCV'95)*, 1995, pp. 816–822.
[10] H. Park, T. Schoepflin, and Y. Kim, "Active contour model with gradient directional information: Directionalsnake," *IEEE Transactions on Circuits and Systems for Video Technology*, vol. 11, no. 2, pp. 252–256, 2001.
[11] J. Garcia-Barnes, D. Rotger, F. Carreras, and et al., "Contrast echography segmentation and tracking by trained deformable models," in *Proc. IEEE Computers in Cariology*, vol. 30, 2003, pp. 173–176.
[12] M. Kass, A. Witkin, and D. Terzopoulos, "Snakes: Active contour models," *Int. J. Comput. Vis.*, vol. 1, no. 4, pp. 321–331, 1988.
[13] T. Cootes, A. Hill, C. Taylor, and J. Haslam, *Information Processing in Medical Imaging*, ser. Lecture Notes in Computer Science. Springer Berlin / Heidelberg, 1993, vol. 687, ch. The use of active shape models for locating structures in medical images, pp. 33–47.
[14] J. Gower, *Generalized procrustes analysis*. Phychometrika, 1975.
[15] J. Garcia-Barnes, D. Gil, S. Pujadas, and F. Carreras, "A variational framework for assessment of the left ventricle motion," *Mathematical Modelling on Natural Phenomena*, vol. 3, pp. 76–100, 2008.